ADVANCED THEORY AND SIMULATIONS
www.advtheorysimul.com

Computational Design of 3D Porous Aluminum Nitride Assembled From AlN-Biphenylene Nanoribbons for Reversible Hydrogen Storage

*Ahmed H. Ati, Jiewei Cheng, Peng-Hu Du, Mohammed M. Obeid, and Qiang Sun**

Hydrogen fuel with zero CO_2 emission is of current interest for global carbon neutralization. In this study, a 3D porous aluminum nitride (*p*-AlN) framework assemble from AlN-biphenylene nanoribbons and investigate its performance in reversible hydrogen storage is presented. Using density functional theory (DFT), it is showed that the *p*-AlN is dynamically and thermally stable, and exhibiting a semiconductor nature with a bandgap of 3.57 eV. The adsorption energy of H_2 is in the range of −0.104 to −0.087 eV/H_2. According to ab initio molecular dynamics (AIMD) simulations, the H_2 molecules remain stable above liquid nitrogen temperature (77 K). The studied system offers gravimetric (volumetric) capacities of 4.95 wt.% (67.86 g L^{-1}) at 77 K/35 bar, and 1.41 wt.% (18.71 g L^{-1}) at 298 K/100 bar, as revealed by grand canonical Monte Carlo (GCMC) simulations based on force field parameters fitted from DFT results.

1. Introduction

The transition from fossil fuels to sustainable energy sources is essential for reducing global CO_2 emissions and mitigating climate change. Hydrogen, recognized for its high energy density and zero carbon emissions, is a key candidate as an energy carrier for future clean energy systems.[1] However, the low gravimetric and volumetric energy densities along with the sluggish kinetic diffusion of H_2 are the major hurdles in developing efficient and safe hydrogen storage systems.[2] Conventional storage methods, such as compressed gas under high pressures (>350 bar) or cryogenic liquid storage at 20 K, are limited by low energy density, high costs, and safety concerns, prompting the need for advanced storage materials that can safely and effectively store hydrogen at practical temperatures and pressures.[3,4] The U.S. Department of Energy (DOE) has set targets of 5.5 wt.% gravimetric and 40 g L^{-1} volumetric capacities for hydrogen storage systems by 2025.[3]

In this regard, storage of hydrogen in solid state materials offers a promising solution. For example, solid porous materials of current interest[5] such as zeolites,[6] metal-organic frameworks (MOFs),[7] and carbon-based structures[8] are efficient in hydrogen storage due to their tunable properties and large surface areas. However, their performance is often limited by weak physisorption interactions resulting from the low polarizability of H_2 molecules.[9] To enhance H_2 interaction, researchers have explored doping these materials with alkali, alkaline earth, or transition metals (TMs), which improve their chemical activity and create more active sites that strengthen hydrogen adsorption. Doping with TMs can improve the absorption, but the large mass of TM atoms can reduce the gravimetric density. Furthermore, doping can lead to the clustering of TM atoms.[10] Therefore, current techniques for improving the interaction between H_2 and porous materials focus on designing porous materials with intrinsic open metal sites. A recent study discovered that porous TiC_2 has a hydrogen adsorption energy of −0.355 eV/H_2, resulting in a storage capacity of 4.0 wt.% and 106.0 g L^{-1} at 16 bar/230 K. Such a high performance is attributed to the Kubas interaction mechanism.[11] Additionally, NU-2100 ($C_6H_2Cu_2N_6$) recorded adsorption energy of 0.331 eV and a storage capability of 10.4 g L^{-1} at 100 bar/233 K.[12] These findings highlight the potential use of new porous materials with intrinsic open metal sites for hydrogen storage.

Among the studied systems, aluminum (Al^{3+}) -based materials are of special interest.[13–15] Al is known for being lightweight, inexpensive, and abundant, making it an attractive option in hydrogen storage applications. Wang et al. have explored the potential in the AlN-based nanostructures in various forms, including nanocages, nanocones, nanotubes, and nanowires. In these structures, the Al site can bind one hydrogen molecule through charge polarization with an adsorption energy of −0.2 eV/H_2 and a capacity of 4.7 wt.%.[16] In nanoporous materials, for example, Al(OH)(O_2C-C_6H_4-CO_2), the storage capacity can reach to 3.8 wt.% at 1.6 MPa/77 K.[17] Additionally, Evans et al. experimentally studied aluminum formate (Al ($HCOO)_3$), known as ALF, which offers adsorption energy of 0.089 eV, and can uptake 12 g H_2/kg of the ALF at 25 bar/120 K.[18] Moreover, the ultraporous MOF NU-1501-Al, designed using simulation-motivated synthesis,

A. H. Ati, J. Cheng, P.-H. Du, M. M. Obeid, Q. Sun
School of Materials Science and Engineering
Peking University
Beijing 100871, China
E-mail: sunqiang@pku.edu.cn
M. M. Obeid
College of Engineering and Engineering Technologies
Al-Mustaqbal University
Babylon 51001, Iraq

The ORCID identification number(s) for the author(s) of this article can be found under https://doi.org/10.1002/adts.202401402

DOI: 10.1002/adts.202401402

exhibits a high storage capacity of 14.0 wt.% (46.2 g L^{-1}) at 100 bar/77 K, due to its low density and large surface area.[19]

To further expand the Al-based materials family for hydrogen storage, we present a computational investigation of a 3D porous aluminum nitride (*p*-AlN) structure based on AlN nanoribbons that feature a biphenylene-like network.[20] Our study focuses on two questions: (1) Can an Al site bind more than one hydrogen molecule? (2) How does the storage capacity change with thermodynamic conditions, and can *p*-AlN exceed the capacity of MOF NU-1501-Al[19]? If so, what factors contribute to this potential improvement? To address these questions, we employed density functional theory (DFT), *ab* initio molecular dynamics (AIMD), and grand canonical Monte Carlo (GCMC) simulations, to analyze the crystal geometry, electronic structures, and hydrogen adsorption capabilities of *p*-AlN.

2. Computational Methods

Calculations are based on density functional theory with the Perdew-Burke-Ernzerhof (PBE) exchange-correlation energy in the generalized gradient approximation (GGA),[21] and van der Waals correction (PBE-D3) to consider van der Waals interactions,[22] as implemented in the Vienna Ab initio Simulation Package (VASP).[23] A plane-wave cutoff energy of 520 eV is used for all calculations. The Brillouin zone is represented by a 2 × 2 × 6 k-mesh with a Gamma scheme. The full geometrical relaxation is performed based on the conjugated-gradient algorithm with a force of $10^{-,3}$ eV $Å^{-1}$ and a total energy of $10^{-,6}$ eV. The dynamical stability of the optimized structure in a 1 × 1 × 3 supercell was validated by phonon spectrum with finite displacements using the Phonopy package.[24] The Heyd-Scuseria-Ernzerhof (HSE06) hybrid scheme is employed to address the issue of underestimating the electronic band structure.[25] An ab initio molecular dynamics (AIMD) simulation is used to confirm the thermal stability of the proposed structure with the canonical (NVT) ensemble using Nose´-Hoover thermostat.[26] The AIMD simulation is performed with 1 × 1 × 3 supercells at 300 K for pristine *p*-AlN and at 77 and 150 K with adsorbed H_2 molecules for 5 ps with a time step of 1 fs.

The cohesive energy of the *p*-AlN is calculated by using the following formula:

$$E_{coh} = \left(xE_{Al} + yE_N - E_{(Al24N24)}\right) / (x + y) \quad (1)$$

Here, E_{Al} and E_{Al} are the energies of isolated Al and N atoms, $E_{(Al24N24)}$ is the total energy of the *p*-AlN system, and *x* and *y* represent the number of Al and N atoms in the *p*-AlN system, respectively.

The adsorption energy (E_{ads}) of H_2 molecules is calculated using the following equation:

$$E_{ads} = \frac{E_{nH_2@AlN} - E_{AlN} - nE_{H_2}}{n} \quad (2)$$

where E_{AlN} is the total energy of the *p*-AlN structure, $E_{nH_2@AlN}$ is the total energy after the adsorption of nH_2 molecules, and E_{H_2} is the energy of a free H_2 molecule.

To evaluate the performance of hydrogen storage materials, the gravimetric (G_c) and volumetric (V_c) capacities are calculated using the following formulas:

$$G_c = \left[\frac{nm_{H_2}}{nm_{H_2} + m_{AlN}}\right] \times 100\% \quad (3)$$

$$V_c = \frac{nm_{H_2}}{V_{sys}} \quad (4)$$

where m_{H_2} and m_{AlN} are the masses of adsorbed H_2 molecules and the AlN system, and V_{sys} is the total volume of the *p*-AlN.

To optimize hydrogen storage materials, it is crucial to understand how temperature and pressure influence hydrogen adsorption. We calculate the desorption temperature using the Van't Hoff equation[27]:

$$T_d = \frac{|E_{ads}|}{k_B}\left[\frac{\Delta S}{R} - \ln(P)\right]^{-1} \quad (5)$$

where k_B is the Boltzmann constant ($1.38 \times 10^{-,23}$ J K^{-1}), ΔS represents the entropy change of H_2 from gas to liquid phase (75.44 J $mol^{-1}.K^{-1}$),[11,28,29] *R* is the gas constant (8.314 J $mol^{-1}.K^{-1}$), and *P* is the equilibrium pressure set at 1 atm.

We performed grand canonical Monte Carlo (GCMC) simulations by using the RASPA 2.0 package,[30] to investigate the adsorption isotherms of H_2 molecules in the *p*-AlN. The accuracy of these simulations relies on the structural integrity of the porous crystal and the selected interatomic potentials.[31] So that to model H_2–H_2 interactions, we employ the YZ LJ-2S mode,[32,33] while the non-bonded interactions between H_2 and *p*-AlN are described using the Morse potential, based on DFT adsorption energies. We explore the potential energy landscape by randomly placing a hydrogen molecule in a 1 × 1 × 2 supercell of *p*-AlN and optimizing its position over 30 steps, and keeping the *p*-AlN atoms fixed. This method allowed us to accurately fit the Morse potential between the center of the hydrogen molecule (H_{com}) and the porous atoms from 955 configurations.

$$U_{ij} = \varepsilon_{ij}\left[\left(1 - e^{-k(r_{ij}-\sigma)}\right)^2 - 1\right] \quad (6)$$

here, ε_{ij}, and *k* define as the depth and width of the potential well, respectively, while r_{ij} is the interaction distance, and σ is the distance at which the potential energy is zero. We used a force field cutoff of 12.8 Å for interactions and employed Ewald summation methods to accurately compute Coulomb potentials.[34] Each simulation consists of 5000 equilibration cycles followed by 5000 production cycles. During these cycles, Monte Carlo moves including insertion, deletion, translation, rotation, and re-insertion are employed. The number of Monte Carlo moves (N) for each cycle is determined by taking the larger value between 20 and the total number of adsorbent molecules.

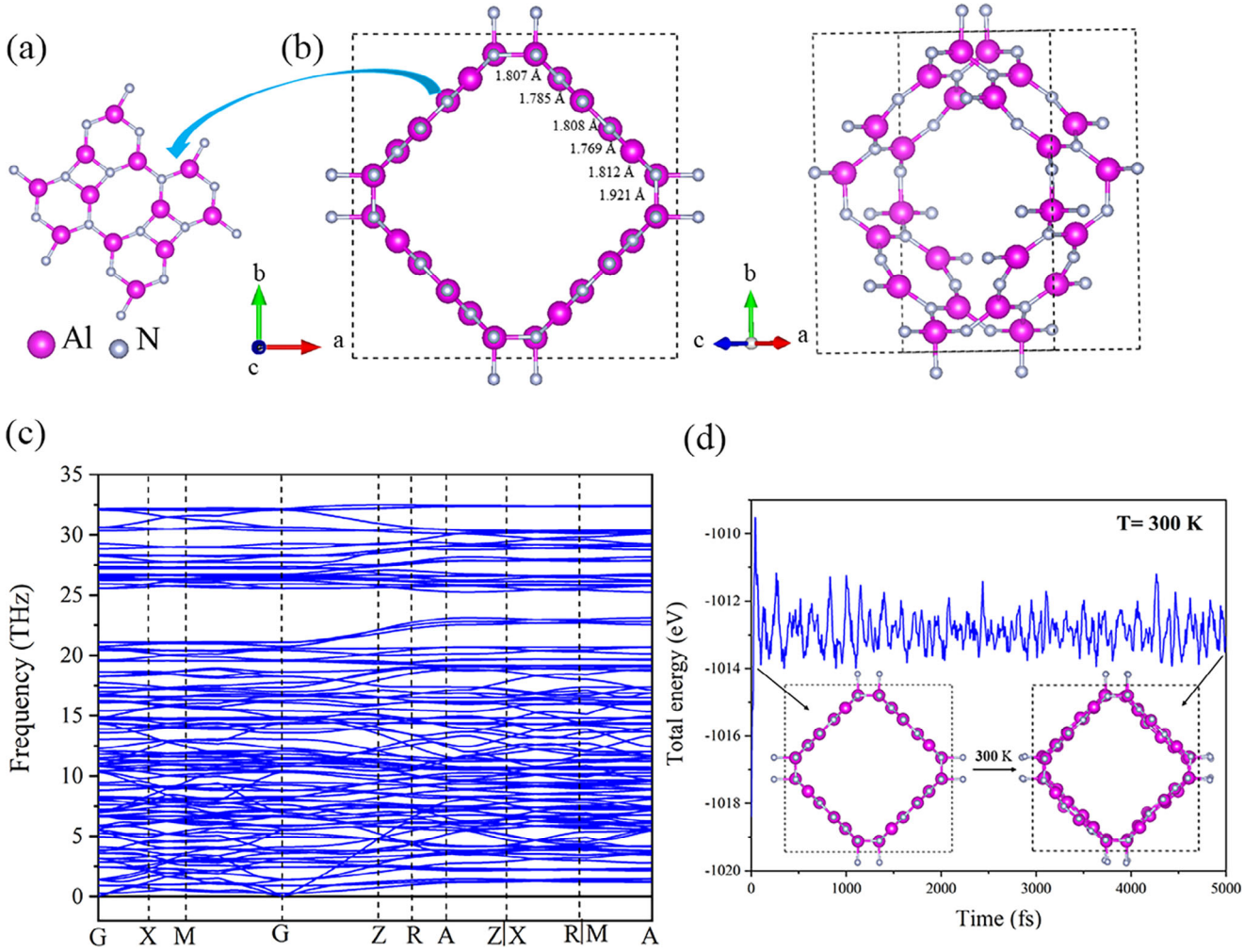

Figure 1. a) AlN nanoribbons as building units, b) unit cell of *p*-AlN, c) phonon spectrum, and d) potential energy fluctuation during AIMD simulations at room temperature.

3. Results and Discussion

3.1. Structure and Stability

Since Fan et al. successfully fabricated an ultraflat biphenylene carbon sheet in (2021),[20] researchers have designed 2D-AlN and conducted theoretical studies to explore its properties. Based on this, we designed the *p*-AlN structure, which is assembled from AlN nanoribbons as building blocks to form a 3D framework. The unit cell with lattice constants a = b = 14.982 Å, and c = 5.592 Å comprises $Al_{24}N_{24}$ atoms with a *P4/nbm* symmetry group (no. 125). Each Al and N atoms have 3 inequivalent sites in the structure (Table S1, Supporting Information). The optimized bond lengths for *p*-AlN are illustrated in (**Figure 1b**). The *p*-AlN structure has a density of 1.301 g cm^{-3} and a pore size of 11.298 Å, making it suitable for hydrogen storage, as experimental results show that storage capacity is limited when pore sizes exceed 1.5 nm.[35]

The stability of sorbent materials is crucial for effective hydrogen storage, as it directly affects the system's structural integrity and adsorption capacity. To evaluate the energetic stability of *p*-AlN, we calculate its cohesive energy, which is 5.40 eV $atom^{-1}$. This value is comparable with that of other AlN structures, including 5.89 eV $atom^{-1}$ for the 2D AlN-biphenylene sheet,[36] 5.76, 5.759, and 5.497 eV $atom^{-1}$ for wurtzite, zinc-blende, and rocksalt phases of bulk AlN, respectively.[37] Additionally, we assessed the dynamical stability by calculating phonon dispersions, which revealed no negative frequency (Figure 1c), confirming it is dynamically stable. Furthermore, we assess the thermal stability of *p*-AlN through AIMD simulations using a 1 × 1 × 3 supercell with 144 atoms to minimize lattice translational constraints. The fluctuation of total potential energy over time is shown in (Figure 1d), which indicates that *p*-AlN remains stable at room temperature (300 K) as the potential energy fluctuates around a constant level and the structure is almost intact.

3.2. Electronic Properties

To explore the electronic properties of the *p*-AlN, we calculated the electronic band structure using HSE06 hybrid functional (**Figure 2a**). The results revealed a direct band gap of 3.57 eV at

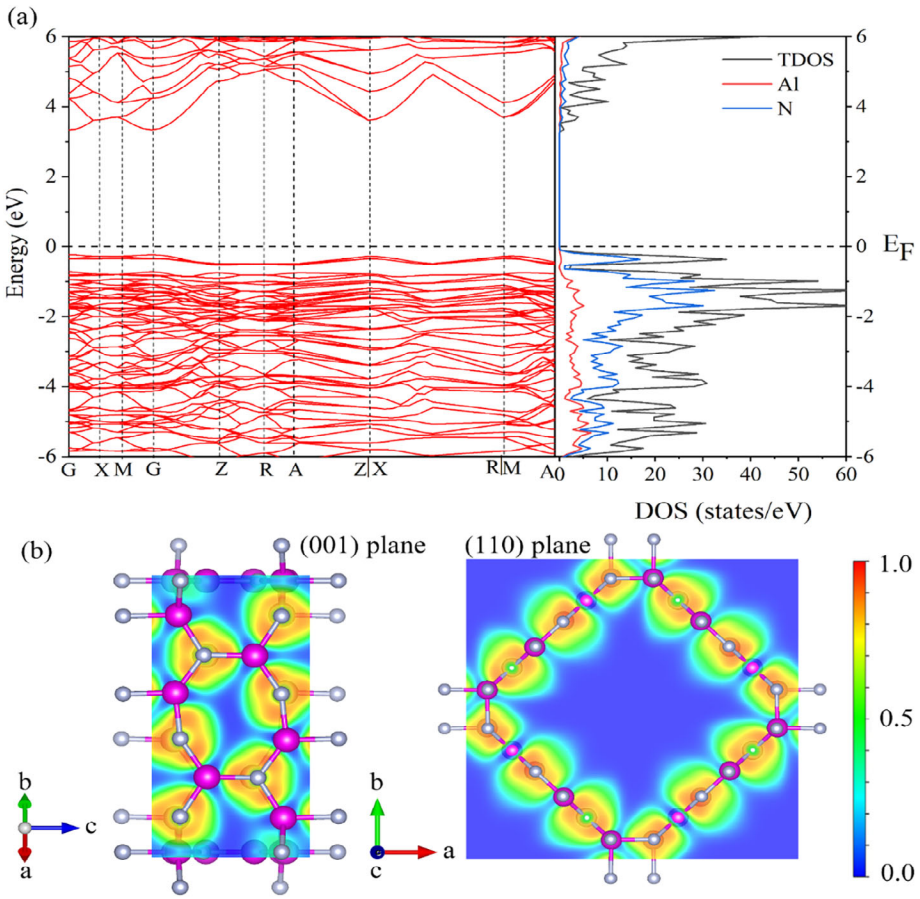

Figure 2. a) Electronic band structure and projected density of states (PDOS) for Al and N atoms in *p*-AlN, calculated with HSE06 hybrid functional. b) Electron localization function (ELF) distribution across two slices of the *p*-AlN.

Γ point, confirming the semiconducting nature of the system, which is higher than that of 3D porous of h-BC_2N (0.43 eV),[38] lz1-BN (0.80 eV),[39] and penta-MgN_8 (1.35 eV),[28] as well as higher from than that of 2D AlN-based biphenylene (3.2 eV).[36] The projected density of states (PDOS) analysis indicated that N, with 5 valence electrons, contributes more to the electronic states near the Fermi level than Al with 3 valence electrons. To investigate the bonding characteristics in *p*-AlN, we analyzed the electron localization function (ELF), as shown in Figure 2b. The ELF values range from 0.0 to 1.0, with 0.0 indicating low electron density, 1.0 representing fully localized electrons, and 0.5 suggesting metallic bonding. Our analysis shows that the ELF values between Al-N pairs in *p*-AlN are above 0.6, confirming the feature of ionic bonding. On the other hand, the electron density difference, as shown in Figure S1 (Supporting Information), and Bader charge analysis clearly support the ionic bond between Al and N atoms. The Bader analysis shows that 2.22 electrons are transferred from each Al atom to the N atom, confirming this bonding nature.

3.3. Hydrogen Storage in *p*-AlN

The ability of a material to store hydrogen depends on its capacity to adsorb H_2 molecules. In our study, we considered two configurations: B1 (each Al site adsorbing one H_2 molecule), and B2 (each Al site adsorbing 1.5 H_2 molecules), as shown in **Figure 3**. After relaxation, the average Al–H_2 distances were 3.020 Å for B1 and 3.235 Å for B2 configurations. The calculated adsorption energies are −0.104 eV/H_2 for B1 and −0.087 eV/H_2 for B2, suggesting weak physisorption dominated by van der Waals forces. These findings suggest that Al sites can indeed bind more than one hydrogen molecule, which is primarily attributed to the pore size effects and framework topology of *p*-AlN. However, it is higher than the experimental work of ALF, which has an adsorption energy of 0.089 eV.[18]

The gravimetric capacity (G_c) and volumetric capacity (V_c) are two key parameters for assessing the performance of the hydrogen storage materials. In the B1 configuration, G_c is 4.68 wt.%, and V_c is 63.98 g L^{-1}. The B2 configuration shows an improvement, with G_c increasing to 6.87 wt.%, and V_c rising to 95.51 g L^{-1}.

The desorption temperature (T_d) is essential for hydrogen storage in solid materials because it directly impacts the efficiency of hydrogen release. For the B1 and B2 configurations in *p*-AlN, the average T_d at 1 atm pressure is 133 and 111 K, respectively. This means that hydrogen can be released at temperatures above these values. Notably, both configurations exceed the boiling point of liquid nitrogen (77 K).

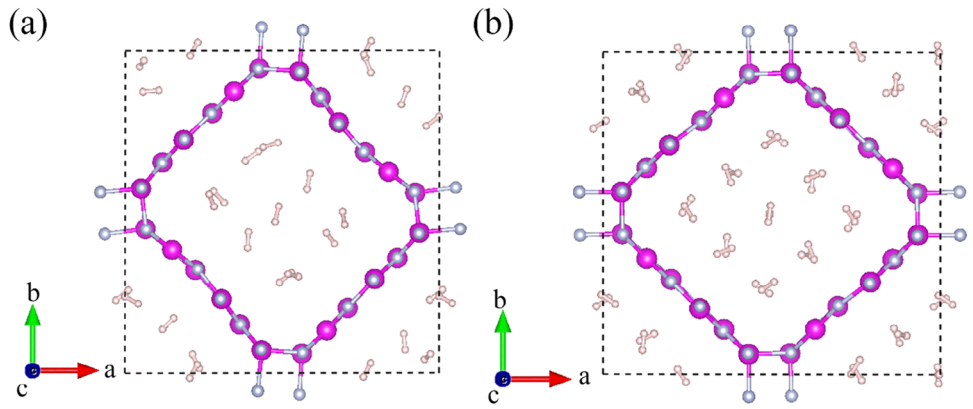

Figure 3. Optimized configuration of H_2 adsorption in *p*-AlN with ratio: a) $1H_2$ for B1 configuration, and b) $1.5H_2$ for B2 configuration.

AIMD simulations are performed for evaluating the hydrogen storage capabilities of materials by examining how H_2 molecules behave under various conditions. For effective hydrogen storage, it is important that H_2 molecules remain stably adsorbed at room temperature or at liquid nitrogen temperature, while also allowing for controlled desorption at higher temperatures. At 77 K, all H_2 molecules remain adsorbed on *p*-AlN after 5 ps, see (**Figure** 4a,c), which is advantageous for efficient hydrogen storage. In contrast, at 150 K, some H_2 molecules begin to desorb (Figure 4b,d), demonstrating the system's ability to facilitate controlled hydrogen release when needed.

GCMC simulations are conducted to study the adsorption of H_2 in *p*-AlN at various pressures and temperatures. To derive the interaction parameters between H_2 and *p*-AlN, we fitted the Morse potential to DFT data, as detailed in **Table** 1. The *p*-AlN consists of six distinct atom types: Al1, Al2, Al3, N1, N2, and

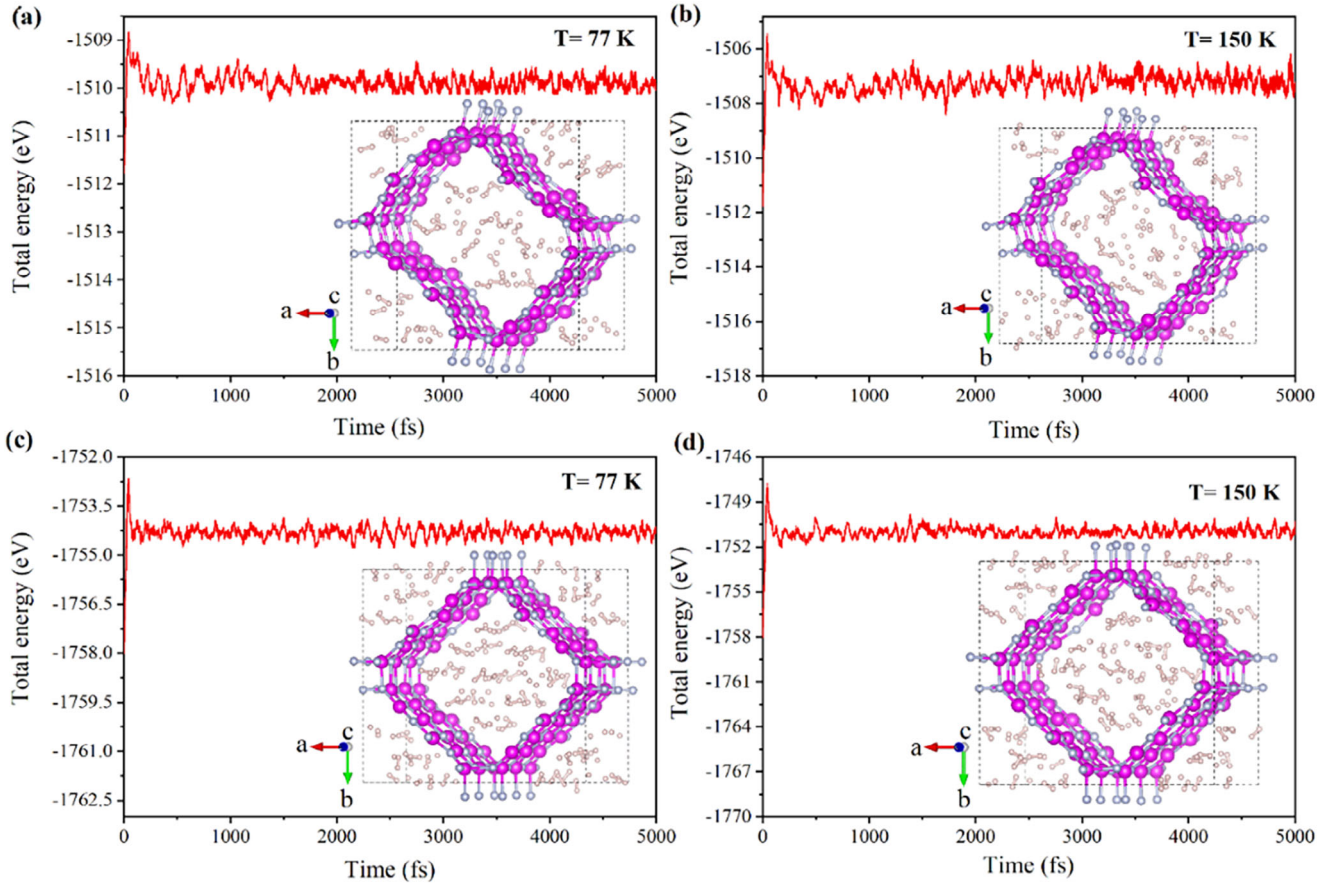

Figure 4. AIMD simulation snapshots of H_2 adsorption in *p*-AlN at 77 and 150 K. It illustrates the total energy fluctuations for two configurations: a,b) B1 configuration with a single H_2 molecule, and c,d) B2 configuration with 1.5 H_2 molecules.

Table 1. Fitted parameters of Morse potential for interaction between H_2 and *p*-AlN.

term H_{com}-	ϵ (K)	k [Å^{-1}]	σ [Å]
Al1	182.637	1.3279	3.8782
Al2	1417.2622	3.2936	2.1176
Al3	1075.6919	6.2064	2.5142
N1	107.8007	1.3899	3.8707
N2	53.2964	0.4889	4.6786
N3	3.9255	2.6233	3.8846

Table 2. Comparison of gravimetric storage capacity of *p*-AlN with some porous materials including Al in the structure under different conditions.

System	Ref	G_c [wt.%]	T[K]	P [bar]
ALF	[18]	1.20	120	25
Al (OH) (O_2C-C_6H_4-CO_2)	[17]	3.80	77	16
CYCU-3	[40]	1.64	77	100
MIL-120	[41]	1.30	77	30
MIL-96	[42]	1.91	77	3.0
AlN	this work	4.95	77	35

N3, illustrated in (**Figure** 5a). The fitting of the Morse potential yielded a high coefficient of determination (R^2 = 0.82) and a low mean absolute error (MAE = 0.12 kcal mol^{-1}), as shown in (Figure 5b).

The H_2 adsorption isotherms of *p*-AlN at 77, 150, and 298 K as a function of pressure are shown in (Figure 5c,d). The highest predicted excess gravimetric (volumetric) capacities 4.95 wt.% (67.86 g L^{-1}) at 77 K/35 bar, and 1.41 wt.% (18.71 g L^{-1}) at 298 K/100 bar. The low adsorption energy of *p*-AlN limits its effectiveness for hydrogen storage at near-ambient temperatures. As temperatures rise, H_2 molecules are released from *p*-AlN, leading to a decrease in its storage capacity. The gravimetric capacity of *p*-AlN was compared to other porous materials containing Al, as listed in **Table** 2. However, the higher density of *p*-AlN (1.301 g cm^{-3}) results in lower hydrogen storage capacities compared to NU-1500-Al (0.498 g cm^{-3}), which stores 8.2 wt.% (44.6 g L^{-1}), and NU-1501-Al (0.283 g cm^{-3}), which stores 14.0 wt.% (46.2 g L^{-1}) at 77 K/100 bar.[19] This demonstrates the influence of framework density on the hydrogen storage capacity of these materials comparable to *p*-AlN.

Furthermore, we tested the reliability of the 5000 cycles by increasing the equilibration and production cycles to 10 000 (Figure S2, Supporting Information), and the results are identical to those obtained at 5000 cycles (Figure 5c,d), confirming that the system has reached equilibrium at 5000 cycles

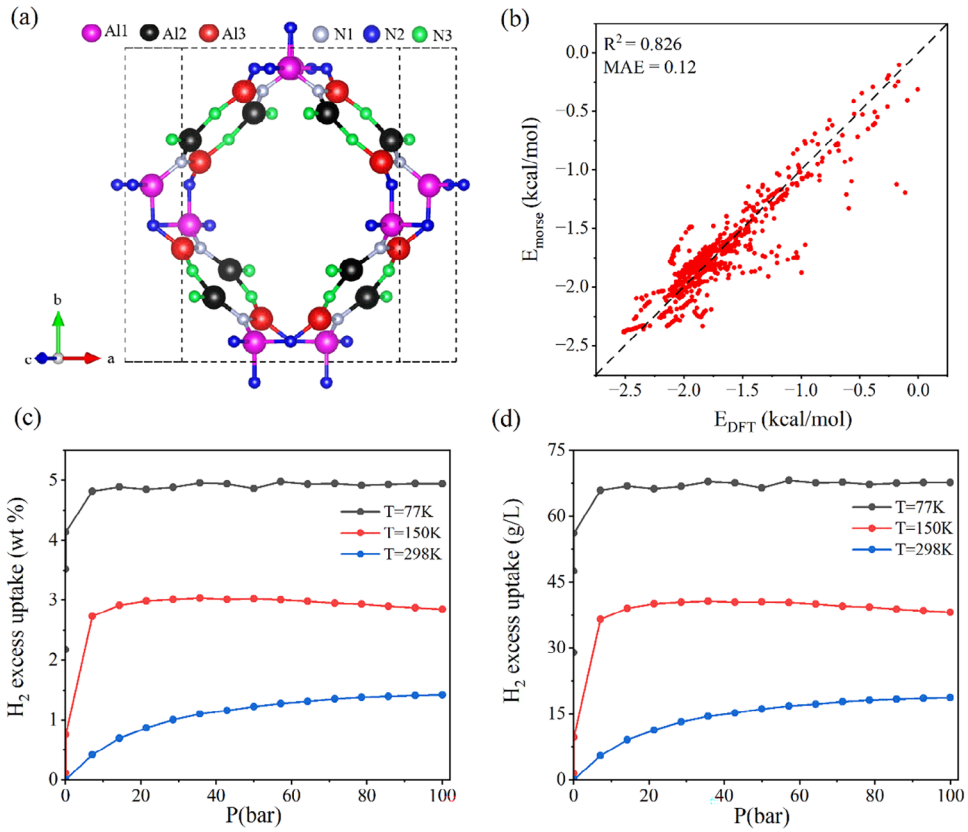

Figure 5. a) Crystal structure with six distinct Al and N sites, b) Comparison of Morse potential energies with DFT energies, and c) and d) Gravimetric and volumetric densities of H_2 adsorption isotherms at 77, 150, and 298 K. These densities were calculated using GCMC simulations based on the Morse force field potential with 5000 cycles.

4. Conclusion

In summary, we investigated the hydrogen storage performance of 3D porous *p*-AlN assembled from AlN-biphenylene nanoribbons. The resulting structure with a band gap of 3.57 eV is found to be dynamically and thermally stable. The adsorption energy of H_2 on Al sites is in the range of −0.104 to −0.087 eV/H_2. AIMD simulations demonstrated stable behavior of H_2 molecules during adsorption and desorption at 77 K. Using DFT-derived force fields, GCMC simulations are carried out for assessing hydrogen storage capabilities at various pressures and temperatures (77, 150, and 298 K), our results show gravimetric (volumetric) capacities of 4.95 wt.% (67.86g L^{-1}) at 77 K/35 bar, and 1.41 wt.% (18.71 g L^{-1}) at 298 K/100 bar. These findings suggest that porous -AlN structures have the potential to serve as promising materials for hydrogen storage applications.

Supporting Information

Supporting Information is available from the Wiley Online Library or from the author.

Acknowledgements

This work was partially supported by grants from the National Key Research and Development Program of China (2021YFB4000601), the National Natural Science Foundation of China [22373005 and 92372112], and the China Scholarship Council (CSC). The calculations were supported by the High-performance Computing Platform of Peking University.

Conflict of Interest

The authors declare no conflict of interest.

Data Availability Statement

The data that support the findings of this study are available from the corresponding author upon reasonable request.

Keywords

3D porous AlN, ab initio molecular dynamics, AlN nanoribbon assembly, density functional theory, Grand Canonical Monte Carlo, hydrogen storage

Received: November 26, 2024
Revised: February 14, 2025
Published online:

[1] S. J. Davis, N. S. Lewis, M. Shaner, S. Aggarwal, D. Arent, I. L. Azevedo, S. M. Benson, T. Bradley, J. Brouwer, Y.-M. Chiang, C. T. M. Clack, A. Cohen, S. Doig, J. Edmonds, P. Fennell, C. B. Field, B. Hannegan, B.-M. Hodge, M. I. Hoffert, E. Ingersoll, P. Jaramillo, K. S. Lackner, K. J. Mach, M. Mastrandrea, J. Ogden, P. F. Peterson, D. L. Sanchez, D. Sperling, J. Stagner, J. E. Trancik, et al., *Science* **2018**, *360*, eaas9793.
[2] J. K. Dawson, *Nature* **1974**, *249*, 724.
[3] A. Schneemann, J. L. White, S. Kang, S. Jeong, L. F. Wan, E. S. Cho, T. W. Heo, D. Prendergast, J. J. Urban, B. C. Wood, M. D. Allendorf, V. Stavila, *Chem. Rev.* **2018**, *118*, 10775.
[4] L. Schlapbach, A. Züttel, *Nature* **2001**, *414*, 353.
[5] Z. Chen, K. O. Kirlikovali, K. B. Idrees, M. C. Wasson, O. K. Farha, *Chem* **2022**, *8*, 693.
[6] P. A. Anderson, in *Solid-State Hydrogen Storage*, (Ed: G. Walker), Woodhead Publishing, England, UK **2008**.
[7] Y. H. Hu, L. Zhang, *Adv. Mater.* **2010**, *22*, E117.
[8] Y. Yürüm, A. Taralp, T. N. Veziroglu, *Int. J. Hydrogen Energy* **2009**, *34*, 3784.
[9] X. Zhou, J. Zhou, Q. Sun, *Front. Phys.* **2011**, *6*, 220.
[10] Q. Sun, Q. Wang, P. Jena, Y. Kawazoe, *J. Am. Chem. Soc.* **2005**, *127*, 14582.
[11] J. Cheng, A. H. Ati, Y. Kawazoe, Q. Sun, *J. Am. Chem. Soc.* **2024**, *146*, 24553.
[12] D. Sengupta, P. Melix, S. Bose, J. Duncan, X. Wang, M. R. Mian, K. O. Kirlikovali, F. Joodaki, T. Islamoglu, T. Yildirim, R. Q. Snurr, O. K. Farha, *J. Am. Chem. Soc.* **2023**, *145*, 20492.
[13] Z. Ao, S. Dou, Z. Xu, Q. Jiang, G. Wang, *Int. J. Hydrogen Energy* **2014**, *39*, 16244.
[14] Z. M. Ao, Q. Jiang, R. Q. Zhang, T. T. Tan, S. Li, *J. Appl. Phys.* **2009**, *105*, 074307.
[15] Z. M. Ao, F. M. Peeters, *Phys. Rev. B* **2010**, *81*, 205406.
[16] Q. Wang, Q. Sun, P. Jena, Y. Kawazoe, *ACS Nano* **2009**, *3*, 621.
[17] G. Férey, M. Latroche, C. Serre, F. Millange, T. Loiseau, A. Percheron-Guégan, *Chem. Commun.* **2003**, 2976.
[18] H. A. Evans, T. Yildirim, P. Peng, Y. Cheng, Z. Deng, Q. Zhang, D. Mullangi, D. Zhao, P. Canepa, H. M. Breunig, A. K. Cheetham, C. M. Brown, *J. Am. Chem. Soc.* **2023**, *145*, 22150.
[19] Z. Chen, P. Li, R. Anderson, X. Wang, X. Zhang, L. Robison, L. R. Redfern, S. Moribe, T. Islamoglu, D. A. Gómez-Gualdrón, T. Yildirim, J. F. Stoddart, O. K. Farha, *Science* **2020**, *368*, 297.
[20] Q. Fan, L. Yan, M. W. Tripp, O. Krejčí, S. Dimosthenous, S. R. Kachel, M. Chen, A. S. Foster, U. Koert, P. Liljeroth, J. M. Gottfried, *Science* **2021**, *372*, 852.
[21] J. P. Perdew, K. Burke, M. Ernzerhof, *Phys. Rev. Lett.* **1996**, *77*, 3865.
[22] S. Grimme, J. Antony, S. Ehrlich, H. Krieg, *J. Chem. Phys.* **2010**, *132*, 154104.
[23] G. Kresse, J. Furthmüller, *Phys. Rev. B* **1996**, *54*, 11169.
[24] A. Togo, I. Tanaka, *Scr. Mater.* **2015**, *108*, 1.
[25] J. Heyd, G. E. Scuseria, M. Ernzerhof, *J. Chem. Phys.* **2003**, *118*, 8207.
[26] S. Nosé, *J. Chem. Phys.* **1984**, *81*, 511.
[27] E. Durgun, S. Ciraci, T. Yildirim, *Phys. Rev. B* **2008**, *77*, 085405.
[28] A. H. Ati, P.-H. Du, M. M. Obeid, J. Cheng, Q. Sun, *ACS Appl. Mater. Interfaces* **2024**, *16*, 27311.
[29] P. Mishra, D. Singh, Y. Sonvane, R. Ahuja, *J. Appl. Phys.* **2020**, *127*, 184305.
[30] D. Dubbeldam, S. Calero, D. E. Ellis, R. Q. Snurr, *Mol. Simul.* **2016**, *42*, 81.
[31] R. B. Getman, Y.-S. Bae, C. E. Wilmer, R. Q. Snurr, *Chem. Rev.* **2012**, *112*, 703.
[32] M. Barraco, S. Neyertz, N. E. Benes, D. Brown, *The Journal of Physical Chemistry A* **2023**, *127*, 6335.
[33] Q. Yang, C. Zhong, *J. Phys. Chem. B* **2005**, *109*, 11862.
[34] P. P. Ewald, *Ann. Phys.* **1921**, *369*, 253.
[35] Y. Gogotsi, C. Portet, S. Osswald, J. M. Simmons, T. Yildirim, G. Laudisio, J. E. Fischer, *Int. J. Hydrogen Energy* **2009**, *34*, 6314.
[36] K. A. Lopes Lima, L. A. Ribeiro, *Mater. Today Commun.* **2023**, *37*, 107183.
[37] P. Vashishta, R. K. Kalia, A. Nakano, J. P. Rino, *J. Appl. Phys.* **2011**, *109*, 033514.

[38] L. Li, X. Li, X. Li, H. Chen, H. Liu, J. Chen, Y. Zhang, *J. Phys. Chem. Lett.* **2022**, *13*, 2348.
[39] N. Khossossi, D. Singh, W. Luo, R. Ahuja, *Electrochim. Acta* **2022**, *421*, 140491.
[40] S.-H. Lo, C.-H. Chien, Y.-L. Lai, C.-C. Yang, J. J. Lee, D. S. Raja, C.-H. Lin, *J. Mater. Chem. A* **2013**, *1*, 324.
[41] C. Volkringer, T. Loiseau, M. Haouas, F. Taulelle, D. Popov, M. Burghammer, C. Riekel, C. Zlotea, F. Cuevas, M. Latroche, D. Phanon, C. Knöfelv, P. L. Llewellyn, G. Férey, *Chem. Mater.* **2009**, *21*, 5783.
[42] T. Loiseau, L. Lecroq, C. Volkringer, J. Marrot, G. Férey, M. Haouas, F. Taulelle, S. Bourrelly, P. L. Llewellyn, M. Latroche, *J. Am. Chem. Soc.* **2006**, *128*, 10223.